

# Thin-film models for viscoelastic liquid bi-layers

Sebastian Jachalski<sup>§</sup>    Andreas Münch<sup>‡</sup>    Barbara Wagner<sup>†§</sup>

February 4, 2016

## Abstract

In this work we consider a two-layer system of viscoelastic liquids of corotational Jeffreys' type dewetting from a Newtonian liquid substrates. We derive conditions that allow for the first time the asymptotically consistent reduction of the free boundary problem for the two-layer system to a system of coupled thin-film equations that incorporate the full nonlinear viscoelastic rheology. We show that these conditions are controlled by the order of magnitude of the viscosity ratio of the liquid layers and their thickness ratio. For pure Newtonian flow, these conditions lead to a thin-film model that couples a layer with a parabolic flow field to a layer described by elongational flow. For this system we establish asymptotic regimes that relate the viscosity ratio to a corresponding apparent slip. We then use numerical simulations to discuss the characteristic morphological and dynamical properties of viscoelastic films of corotational Jeffreys' type dewetting from a solid as well as liquid substrate.

**Key words.** Fluid dynamics; Viscoelasticity; Thin-film models; Two-phase flow; Asymptotic Methods; Numerical Solution

## 1 Introduction

Liquid two-layer systems frequently combine layers of different rheological and interfacial properties to be exploited in nature and in various technological applications, for example for process engineering organic photovoltaics devices or similar processes used in the semi-conductor industry [4, 14, 20, 25, 27]. For many of these applications the dimensions, in particular the thickness, of the layers are in the micro- to nanometer range so that rupture and subsequent liquid dewetting become important problems that need to be understood.

The mathematical boundary value problem of the two-layer system governing these processes often involve layers of viscoelastic polymers besides Newtonian liquids, together with free and interfacial boundaries. For two-layer thin films of Newtonian liquids it has been shown in the past that the asymptotic reduction of the governing equations to a system of thin-film models can be achieved via a lubrication type approximation by making use of the scale separation between horizontal and vertical dimensions [1, 10, 17, 23, 28, 35]. The availability of such dimension-reduced models bears great advantages for the analysis and numerical simulation of the underlying free boundary problem and becomes even more important if the focus of interest lies in the formation and design of three-dimensional patterns.

For two-layer systems that incorporate nonlinear viscoelastic rheologies, such as the corotational Jeffreys' model or the better known Oldroyd-B model, similar derivations of thin-film

---

<sup>§</sup>Weierstrass Institute, Mohrenstraße 39, 10117 Berlin, Germany

<sup>‡</sup>Mathematical Institute, University of Oxford, Andrew Wiles Building, Woodstock Road, Oxford, OX2 6GG

<sup>†</sup>Technische Universität Berlin, Institute of Mathematics, Straße des 17. Juni 136, 10623 Berlin, Germany

models have not been investigated so far. In fact, for the simpler situation of the flow of a single liquid layer on a solid substrate an asymptotically consistent derivation of closed form lubrication approximations that incorporate nonlinear viscoelastic rheologies is in general not possible [6, 30, 43]. However, as has been shown in [32], when it is assumed that friction at the boundary with the substrate is reduced by allowing the liquid film to slip along the substrate, then the nonlinear corotational Jeffreys model can be fully incorporated into a thin-film approximation. Specifically, it is shown there that an asymptotically consistent derivation of the thin-film model requires the slip-length to be of order of magnitude much larger than the thickness of the dewetting layer.

In this study we show that for the two-layer system of a nonlinear viscoelastic liquid film dewetting from a liquid substrate an asymptotically consistent thin-film approximation can be obtained if the viscosity of the liquid substrate is much smaller than the one of the dewetting layer. We argue that this regime gives rise to a plug flow in the dewetting layer, so that the normal stresses remain asymptotically consistent with the thin film approximation. In fact, if both layers are Newtonian the analogous conclusion can be drawn, that is, a thin-film equation for plug-flow including extensional stresses is obtained for the dewetting layer.

The connection between low viscosity of the liquid substrate and plug flow in the dewetting layer has already been made by Brochard et al. [8] and Joanny et al. [24] but without taking viscoelastic effects into account. On the other hand, for the single layer situation with slip at the solid substrate, the importance of extensional stresses in plug flow regimes has been explored theoretically and experimentally only recently, for example in [2, 15, 33].

In this work after the formulation of the free boundary problem in Section 2, we combine both ideas to derive a class of thin film models which incorporate also extensional stresses in the thin-film approximation in Section 3. We show transitions in flow regimes by varying the order of magnitude of the viscosity ratios of the liquid layers as well as their thicknesses. We show that these regimes produce characteristic dewetting profiles for the dewetting layer as well as for the interface with the underlying liquid substrate.

For the special case of an undeformable interface with the liquid substrate and for increasing surface tension with the substrate, we show in Section 4 that the transitions in flow regimes and the corresponding surface profiles of the dewetting layer can be brought in one-to-one correspondence with the previously discussed transitions for moderate to large slip boundary conditions, that has been investigated in the past [33]. Finally, in Section 5 we use these results on the flow regimes and profile transitions to study the specific signatures when nonlinear viscoelastic effects of the corotational Jeffreys type and extensional stresses are incorporated in the thin-film approximation to leading order.

## 2 Formulation of the free-boundary problem

Constitutive laws that model the viscoelastic properties of polymer melts such as Polystyrene (PS) or Polydimethylsiloxane (PDMS) often use some form of a generalized Maxwell or Jeffreys model or alternatively, Oldroyd's model, see Hassager et al. [36] for detailed derivations and discussions. In the context of thin-film flows of polymer melts, various viscoelastic models have been discussed in the past, [6, 7, 21, 26, 37, 41] to explain the morphology and other characteristics of dewetting polymer films from a solid substrate. For the study of two-layer liquid systems considered here, we use the corotational Jeffreys model in the governing equations for the upper layer to reflect advective and corotational nonlinearities, while we let the substrate layer obey Newtonian flow behaviour.

The set-up of the liquid-liquid system is shown in the sketch in fig. 1. First, we define two

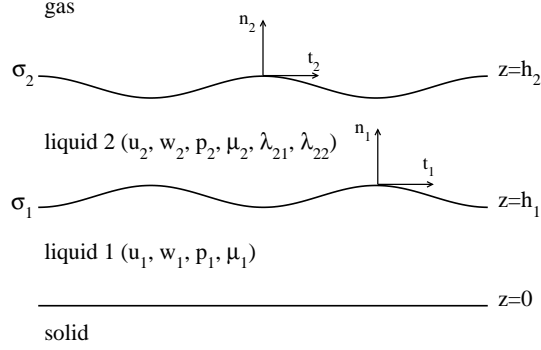


Figure 1: Sketch of the bi-layer system.

82 domains which are occupied by the liquids by

$$\Omega_1 := \{(x, z, t) \mid 0 \leq z \leq h_1(x, t)\}, \quad \Omega_2 := \{(x, z, t) \mid h_1(x, t) \leq z \leq h_2(x, t)\}, \quad (2.1)$$

83 where  $h_1(x, t)$  denotes the interfacial free boundary between the lower and upper liquid layer,  
 84  $h_2(x, t)$  is the free boundary to the ambient gas. From this point on we denote quantities which  
 85 are related to the lower liquid by index 1. Analogously we use index 2 for quantities which are  
 86 related to the upper layer.

87 The governing equations for the evolution of the liquid layers within the domains  $\Omega_1$  and  $\Omega_2$   
 88 are given by the continuity equation for both layers and the Cauchy momentum equations

$$0 = \partial_x u_i + \partial_z w_i, \quad (2.2a)$$

$$\rho_i \frac{d}{dt} u_i = -\partial_x p_i + \partial_x \tau_{i,11} + \partial_z \tau_{i,12}, \quad (2.2b)$$

$$\rho_i \frac{d}{dt} w_i = -\partial_z p_i + \partial_x \tau_{i,12} + \partial_z \tau_{i,22}, \quad (2.2c)$$

89 where  $u_i$  and  $w_i$  denote the velocities in the horizontal and vertical direction, respectively,  $\rho_i$  are  
 90 the densities of the liquid layers and  $p_i$  denote the hydrostatic pressures.

91 In the upper viscoelastic layer we assume that the symmetric stress tensor  $\tau_2$  obeys the  
 92 corotational Jeffreys model with the constitutive equation

$$\tau_2 + \lambda_{21} \frac{D}{Dt} \tau_2 = \mu_2 \left( \dot{\gamma}_2 + \lambda_{22} \frac{D}{Dt} \dot{\gamma}_2 \right), \quad (2.3)$$

93 and where the Jaumann derivative  $D/Dt$  is defined by

$$\frac{D\Lambda}{Dt} = \frac{d\Lambda}{dt} + \frac{1}{2} (\omega_2 \Lambda - \Lambda \omega_2), \quad (2.4)$$

94 for an arbitrary tensor field  $\Lambda$ . The strain rate  $\dot{\gamma}_2$  is given by

$$\dot{\gamma}_2 = \begin{pmatrix} 2\partial_x u_2 & \partial_z u_2 + \partial_x w_2 \\ \partial_z u_2 + \partial_x w_2 & 2\partial_z w_2 \end{pmatrix}, \quad (2.5)$$

95 and the vorticity tensor is

$$\omega_2 = \begin{pmatrix} 0 & \partial_x w_2 - \partial_z u_2 \\ \partial_z u_2 - \partial_x w_2 & 0 \end{pmatrix}. \quad (2.6)$$

96 Since the lower layer is assumed to behave as a Newtonian fluid, the stress tensor  $\tau_1$  is propor-  
97 tional to the strain rate  $\dot{\gamma}_1$ .

$$\tau_1 = \mu_1 \begin{pmatrix} 2\partial_x u_1 & \partial_z u_1 + \partial_x w_1 \\ \partial_z u_1 + \partial_x w_1 & 2\partial_z w_1 \end{pmatrix}. \quad (2.7)$$

98 In this work we assume the viscosities  $\mu_1$  and  $\mu_2$  as well as the relaxation parameters  $\lambda_{21}$  and  $\lambda_{22}$   
99 to be constant material parameters. The relaxation parameter  $\lambda_{21}$  typically denotes a measure  
100 of the time required for the stress to relax to some limiting value, whereas  $\lambda_{22}$  is a measure of  
101 the retardation to return to the equilibrium state, see for example [36].

102 The geometry of the problem yield three boundaries, one at the solid substrate, and two  
103 free boundaries at the liquid-liquid interface and one at the free boundary with the ambient gas  
104 or air. At the solid boundary, which is here at  $z = 0$  we assume no-slip and impermeability  
105 conditions.

$$u_1 = 0, \quad w_1 = 0. \quad (2.8a)$$

106 At the liquid-liquid interface  $z = h_1$  we obtain the kinematic condition

$$\partial_t h_1 = w_1 - \partial_x h_1 u_1, \quad (2.8b)$$

107 Also we assume that the tangential and normal stress force balances

$$(\tau_{1,12} - \tau_{2,12})(1 - (\partial_x h_1)^2) + ((\tau_{1,22} - \tau_{1,11}) - (\tau_{2,22} - \tau_{2,11}))\partial_x h_1 = 0, \quad (2.8c)$$

108 and

$$\begin{aligned} & -p_1 + p_2 - \phi'(h) + \frac{(\tau_{1,11} - \tau_{2,11})(\partial_x h_1)^2 - 2(\tau_{1,12} - \tau_{2,12})\partial_x h_1 + (\tau_{1,22} - \tau_{2,22})}{1 + (\partial_x h_1)^2} \\ & = \sigma_1 \frac{\partial_{xx} h_1}{(1 + (\partial_x h_1)^2)^{3/2}}, \end{aligned} \quad (2.8d)$$

109 are satisfied, respectively, where where  $\phi'(h)$  is a function of the thickness of the top layer  
110  $h := h_2 - h_1$  and denotes the disjoining pressure arising from the intermolecular van der Waals  
111 forces that drive the rupture and subsequent dewetting of the upper layer, combined with a  
112 stabilizing contribution at very small thicknesses arising from Born repulsion forces. A typical  
113 choice for the intermolecular potential  $\phi(h)$  is

$$\phi(h) = \frac{8}{3}\phi_* \left[ \frac{1}{8} \left( \frac{h_*}{h} \right)^8 - \frac{1}{2} \left( \frac{h_*}{h} \right)^2 \right], \quad (2.8e)$$

114 where here the choice of constants is such that  $\phi_* < 0$  is the minimum of the potential at  $h = h_*$ ,  
115 which is the thickness that remains after the film has dewetted, see for example [23].

116 We assume no-slip and impermeability at  $z = h_1$  which yield the corresponding conditions

$$(u_2 - u_1) + (w_2 - w_1)\partial_x h_1 = 0, \quad -(u_2 - u_1)\partial_x h_1 + (w_2 - w_1) = 0. \quad (2.8f)$$

117 Similarly, we obtain for the boundary conditions at the free boundary  $z = h_2$  the kinematic  
118 condition,

$$\partial_t h_2 = w_2 - \partial_x h_2 u_2, \quad (2.8g)$$

119 and the tangential and normal stress force balances

$$\tau_{2,12} (1 - (\partial_x h_2)^2) + (\tau_{2,22} - \tau_{2,11}) \partial_x h_2 = 0, \quad (2.8h)$$

120 and

$$-p_2 + \phi'(h) + \frac{\tau_{2,11}(\partial_x h_2)^2 - 2\tau_{2,12}\partial_x h_2 + \tau_{2,22}}{1 + (\partial_x h_2)^2} = \sigma_2 \frac{\partial_{xx} h_2}{(1 + (\partial_x h_2)^2)^{3/2}}. \quad (2.8i)$$

### 121 3 Thin-film model for the viscoelastic bi-layer

#### 122 3.1 Scaled problem

123 For the nondimensional problem we introduce the following dimensionless quantities

$$x = Lx^*, \quad (z, h_i) = H(z^*, h_i^*), \quad (t, \lambda_{21}, \lambda_{22}) = T(t^*, \lambda_{21}^*), \quad (3.1a)$$

$$(u_1, u_2) = U(u_1^*, u_2^*), \quad (w_1, w_2) = W(w_1^*, w_2^*), \quad (p_i, \phi') = P(p_i^*, \phi'^*), \quad (3.1b)$$

124 where  $L$  and  $H$  denote the characteristic length scales and  $U, W$  the characteristic velocity scales  
125 in the vertical and horizontal direction, respectively. For the stress tensors we set

$$\begin{pmatrix} \tau_{i,11} & \tau_{i,12} \\ \tau_{i,21} & \tau_{i,22} \end{pmatrix} = \frac{\mu_i}{T} \begin{pmatrix} \tau_{i,11}^* & \frac{L}{H} \tau_{i,12}^* \\ \frac{L}{H} \tau_{i,21}^* & \tau_{i,22}^* \end{pmatrix}. \quad (3.2)$$

126 For the system of thin liquid layers the characteristic length scales of the evolving patterns in the  
127 horizontal direction are much larger than the typical scale of the heights  $h_i$ . We thus introduce  
128 the small parameter

$$\varepsilon := \frac{H}{L} = \sqrt{\frac{8\phi^*}{3\sigma_2}} \ll 1 \quad (3.3)$$

129 which is fixed by the pressure scale from the intermolecular potential, i.e.  $P = 8\phi^*/3H$ . In  
130 view of the kinematic conditions determine the timescale via

$$T = \frac{L}{U}, \quad (3.4)$$

131 Balancing the terms in the stress force conditions yields the relations

$$P = \frac{\sigma_2 H}{L^2} \quad \text{and} \quad \frac{\mu_2 U}{\sigma_2} = \varepsilon. \quad (3.5)$$

132 In [32] it has been argued that in order to incorporate the full corotational Jeffreys con-  
133 stitutive law the boundary condition with the substrate needs to allow for large apparent slip  
134 on order of magnitude  $O(\varepsilon^{-2})$ . For liquid two-layer systems we argue here, that an analogous  
135 condition that allows the derivation of a thin-film model and also captures the nonlinear features  
136 of the corotational Jeffreys model, requires the ratio of the viscosities of the two layers to be of  
137 order of magnitude  $O(\varepsilon^{-2})$ .

138 In this case we assume

$$\mu := \frac{\mu_1}{\mu_2} \varepsilon^{-2} = O(1), \quad (3.6)$$

139 keeping the ratio of the surface tensions  $\sigma := \sigma_1/\sigma_2 = O(1)$ .

140 Assuming the relationships in 3.6 we obtain for the non-dimensional equations in the bulk

$$\partial_x u_1 + \partial_z w_1 = 0, \quad \partial_x u_2 + \partial_z w_2 = 0, \quad (3.7a)$$

141

$$0 = -\varepsilon^2 \partial_x p_1 + \varepsilon^4 \mu \partial_{xx} u_1 + \varepsilon^2 \mu \partial_{zz} u_1, \quad (3.7b)$$

$$0 = -\partial_z p_1 + \varepsilon^2 \mu \partial_{xx} w_1 + \varepsilon^2 \mu \partial_{zz} w_1, \quad (3.7c)$$

142

$$0 = -\varepsilon^2 \partial_x p_2 + \varepsilon^2 \partial_x \tau_{2,11} + \partial_z \tau_{2,12}, \quad (3.7d)$$

$$0 = -\partial_z p_2 + \partial_x \tau_{2,12} + \partial_z \tau_{2,22}, \quad (3.7e)$$

143 where the stress tensor of the upper liquids fulfil

$$\begin{aligned} & \left(1 + \lambda_{21} \frac{d}{dt}\right) \tau_{2,11} - \lambda_{21} \left(\frac{1}{\varepsilon^2} \partial_z u_2 - \partial_x w_2\right) \tau_{2,12} \\ &= 2 \left(1 + \lambda_{22} \frac{d}{dt}\right) \partial_x u_2 - \lambda_{22} \left(\left(\frac{1}{\varepsilon} \partial_z u_2\right)^2 - (\varepsilon \partial_x w_2)^2\right), \end{aligned} \quad (3.8a)$$

144

$$\begin{aligned} & \left(1 + \lambda_{21} \frac{d}{dt}\right) \tau_{2,22} + \lambda_{21} \left(\frac{1}{\varepsilon^2} \partial_z u_2 - \partial_x w_2\right) \tau_{2,12} \\ &= 2 \left(1 + \lambda_{22} \frac{d}{dt}\right) \partial_z w_2 + \lambda_{22} \left(\left(\frac{1}{\varepsilon} \partial_z u_2\right)^2 - (\varepsilon \partial_x w_2)^2\right), \end{aligned} \quad (3.8b)$$

145

$$\begin{aligned} & \left(1 + \lambda_{21} \frac{d}{dt}\right) \tau_{2,12} + \frac{\lambda_{21}}{2} (\partial_z u_2 - \varepsilon^2 \partial_x w_2) (\tau_{2,11} - \tau_{2,22}) \\ &= \left(1 + \lambda_{22} \frac{d}{dt}\right) (\partial_z u_2 + \varepsilon^2 \partial_x w_2) + 2\lambda_{22} (\partial_z u_2 - \varepsilon^2 \partial_x w_2) \partial_x u_2. \end{aligned} \quad (3.8c)$$

146 The boundary conditions at  $z = 0$  are

$$u_1 = 0, \quad w_1 = 0. \quad (3.9)$$

147 The equations at  $z = h_1$  become

$$\partial_t h_1 = w_1 - \partial_x h_1 u_1. \quad (3.10)$$

148

$$(\varepsilon^2 \mu (\partial_z u_1 + \varepsilon^2 \partial_x w_1) - \tau_{2,12}) \left(1 - (\varepsilon \partial_x h_1)^2\right) \quad (3.11)$$

$$+ \varepsilon^2 (2\varepsilon^2 \mu (\partial_z w_1 - \partial_x u_1) - (\tau_{2,22} - \tau_{2,11})) \partial_x h_1 = 0, \quad (3.12)$$

149

$$\begin{aligned} & -p_1 + p_2 - \phi'(h) \\ &+ \frac{(2\varepsilon^2 \mu \partial_x u_1 - \tau_{2,11}) (\varepsilon \partial_x h_1)^2 - 2(\varepsilon^2 \mu (\partial_z u_1 + \varepsilon^2 \partial_x w_1) - \tau_{2,12}) \partial_x h_1 + (2\varepsilon^2 \mu \partial_z w_1 - \tau_{2,22})}{1 + (\varepsilon \partial_x h_1)^2} \\ &= \frac{\sigma \partial_{xx} h_1}{(1 + (\varepsilon \partial_x h_1)^2)^{3/2}}, \end{aligned} \quad (3.13)$$

150 and

$$(u_2 - u_1) + \varepsilon^2(w_2 - w_1)\partial_x h_1 = 0, \quad -(u_2 - u_1)\partial_x h_1 + (w_2 - w_1) = 0. \quad (3.14)$$

151 At  $z = h_2$  we obtain

$$\partial_t h_2 = w_2 - \partial_x h_2 u_2. \quad (3.15)$$

152

$$\tau_{2,12} \left(1 - (\varepsilon \partial_x h_2)^2\right) + \varepsilon^2 (\tau_{2,22} - \tau_{2,11}) \partial_x h_2 = 0, \quad (3.16)$$

153 and

$$-p_2 + \phi'(h) + \frac{\tau_{2,11} (\varepsilon \partial_x h_2)^2 - 2\tau_{2,12} \partial_x h_2 + \tau_{2,22}}{1 + (\varepsilon \partial_x h_2)^2} = \frac{\partial_{xx} h_2}{(1 + (\varepsilon \partial_x h_2)^2)^{3/2}}. \quad (3.17)$$

### 154 3.2 Thin-film model

155 We will now show that to leading order in  $\varepsilon$  the free boundary problem can be integrated and  
 156 reduced to a system of coupled partial differential equations for the height  $h$ ,  $h_1$ ,  $u_2$  and  $S$ . To  
 157 leading order the equations in the bulk of the lower liquid and in the upper liquid are

$$\partial_x u_1 + \partial_z w_1 = 0, \quad 0 = -\partial_x p_1 + \mu \partial_{zz} u_1, \quad 0 = -\partial_z p_1 \quad (3.18a)$$

158 and

$$\partial_x u_2 + \partial_z w_2 = 0, \quad 0 = \partial_z \tau_{2,12}, \quad 0 = -\partial_z p_2 + \partial_x \tau_{2,12} + \partial_z \tau_{2,22}, \quad (3.18b)$$

159 where

$$\lambda_{21} \partial_z u_2 \tau_{2,12} = \lambda_{22} (\partial_z u_2)^2 \quad (3.18c)$$

160 and

$$\left(1 + \lambda_{21} \frac{d}{dt}\right) \tau_{2,12} + \frac{\lambda_{21}}{2} \partial_z u_2 (\tau_{2,11} - \tau_{2,22}) = \left(1 + \lambda_{22} \frac{d}{dt}\right) \partial_z u_2 + 2\lambda_{22} \partial_z u_2 \partial_x u_2. \quad (3.18d)$$

161 The boundary conditions are

$$u_1 = 0, \quad w_1 = 0 \quad (3.18e)$$

162 at  $z = 0$ ,

$$\partial_t h_1 = w_1 - \partial_x h_1 u_1, \quad (3.18f)$$

163

$$\tau_{2,12} = 0, \quad -p_1 + p_2 - \phi'(h) - \tau_{2,22} = \sigma \partial_{xx} h_1, \quad (3.18g)$$

164

$$u_2 - u_1 = 0, \quad -(u_2 - u_1)\partial_x h_1 + (w_2 - w_1) = 0, \quad (3.18h)$$

165 at  $z = h_1$  and

$$\partial_t h_2 = w_2 - \partial_x h_2 u_2, \quad (3.18i)$$

166

$$\tau_{2,12} = 0, \quad -p_2 + \phi'(h) + \tau_{2,22} = \partial_{xx}h_2 \quad (3.18j)$$

167 at  $z = h_2$ .

168 In order to obtain a closed set of equation we also need to account for the some relations for  
 169 the stress tensor from the next order problem, where we have expanded the variables  $u_i, w_i, p_i,$   
 170  $\tau_{i,jk}$  with  $i, j, k \in 1, 2$  as  $u_i = u_i^{(0)} + \varepsilon^2 u_i^{(1)} + O(\varepsilon^4)$  and likewise with the other variables. For  
 171 ease of notation we then dropped the  $(0)$  from the leading order variables. The relations we need  
 172 are,

$$0 = -\partial_x p_2 + \partial_x \tau_{2,11} + \partial_z \tau_{2,12}^{(1)}, \quad (3.19a)$$

173

$$\left(1 + \lambda_{21} \frac{d}{dt}\right) \tau_{2,11} = 2 \left(1 + \lambda_{22} \frac{d}{dt}\right) \partial_x u_2, \quad (3.19b)$$

174

$$\left(1 + \lambda_{21} \frac{d}{dt}\right) \tau_{2,22} = 2 \left(1 + \lambda_{22} \frac{d}{dt}\right) \partial_z w_2, \quad (3.19c)$$

175 which hold for  $(x, z, t) \in \Omega_2$  as well as

$$(\mu \partial_z u_1 - \tau_{2,12}^{(1)}) - (\tau_{2,22} - \tau_{2,11}) \partial_x h_1 = 0, \quad (3.19d)$$

176 at  $z = h_1$  and

$$\tau_{2,12}^{(1)} + (\tau_{2,22} - \tau_{2,11}) \partial_x h_2 = 0, \quad (3.19e)$$

177 at  $z = h_2$ .

178 Our first observation is that integration the leading order momentum balance in the upper  
 179 layer (3.18b) w.r.t.  $z$  and using the boundary condition (3.18j) gives

$$p_2 = \tau_{2,22} - \partial_{xx}h_1 - \partial_{xx}h + \phi'(h). \quad (3.20)$$

180 Combining this expression with the next order momentum balance (3.19a) we obtain

$$0 = \partial_x(\partial_{xx}h_1 + \partial_{xx}h - \phi'(h)) + \partial_x(\tau_{2,11} - \tau_{2,22}) + \partial_z \tau_{2,12}^{(1)}. \quad (3.21)$$

181 We set

$$\bar{\tau}_2 := \tau_{2,11} - \tau_{2,22}. \quad (3.22)$$

182 Then integration of equation (3.21) gives

$$0 = h \partial_x(\partial_{xx}h_1 + \partial_{xx}h - \phi'(h)) + \int_{h_1}^{h_2} \partial_x \bar{\tau}_2 dz + \tau_{2,12}^{(1)}|_{z=h_2} - \tau_{2,12}^{(1)}|_{z=h_1}. \quad (3.23)$$

183 If we use this expression together with the next order boundary conditions (3.19d–3.19e) and set

184

$$S := \frac{1}{4h} \int_{h_1}^{h_2} \bar{\tau}_2 dz, \quad (3.24)$$

185 we obtain

$$0 = h \partial_x(\partial_{xx}h_1 + \partial_{xx}h - \phi'(h)) + 4 \partial_x(hS) - \mu \partial_z u_1|_{z=h_1}. \quad (3.25)$$



186 In the next step we derive an equation for  $S$ . We first note that because of (3.18b–3.18c) and  
 187 (3.18g)  $u_2 = u_2(x, t)$  does not depend on  $z$ . We combine (3.19b) and (3.19c) to

$$\left(1 + \lambda_{21} \frac{d}{dt}\right) \bar{\tau}_2 = 4(1 + \lambda_{22} \partial_t + \lambda_{22} u_2 \partial_x) \partial_x u_2. \quad (3.26)$$

188 Integration of the left hand side of this equation yields

$$\int_{h_1}^{h_2} \left(1 + \lambda_{21} \frac{d}{dt}\right) \bar{\tau}_2 dz \quad (3.27)$$

$$= \int_{h_1}^{h_2} (1 + \lambda_{21} \partial_t + \lambda_{21} u_2 \partial_x + \lambda_{21} u_2 \partial_z) \bar{\tau}_2 dz \quad (3.28)$$

$$= \int_{h_1}^{h_2} (1 + \lambda_{21} \partial_t + \lambda_{21} u_2 \partial_x + \lambda_{21} (-z \partial_x u_2 + \partial_t h_1 + \partial_x (u_2 h_1)) \partial_z) \bar{\tau}_2 dz \quad (3.29)$$

$$= 4h(1 + \lambda_{21} \partial_t + \lambda_{21} u_2 \partial_x) S \quad (3.30)$$

189 Hence, we obtain the equation for  $S$

$$(1 + \lambda_{21} \partial_t + \lambda_{21} u_2 \partial_x) S = (1 + \lambda_{22} \partial_t + \lambda_{22} u_2 \partial_x) \partial_x u_2. \quad (3.31)$$

190 The kinematic and impermeability conditions imply the equation for  $h$

$$\partial_t h = -\partial_x (h u_2). \quad (3.32)$$

191 In the last step we consider the evolution of the lower fluid and the interface  $h_1$ . From (3.18a)  
 192 and (3.18e) we first obtain

$$u_1 = \frac{1}{2\mu} \partial_x p_1 z^2 + c z, \quad (3.33)$$

193 which we use for the evolution equation for  $h_1$

$$\partial_t h_1 = -\partial_x \int_0^{h_1} u_1 dz = -\partial_x \left( \frac{1}{6\mu} h_1^3 \partial_x p_1 + \frac{1}{2} h_1^2 c \right). \quad (3.34)$$

194 and determine the constant  $c$  from equation

$$\frac{1}{2\mu} \partial_x p_1 h_1^2 + c h_1 = u_2 \quad (3.35)$$

195 and by using (3.18h). We finally obtain the closed system of equations for  $h_1$ ,  $h$ ,  $S$  and  $u_2$ .

$$\partial_t h = -\partial_x (h u_2), \quad (3.36a)$$

$$\partial_t h_1 = \frac{1}{12\mu} \partial_x (h_1^3 \partial_x p_1) - \frac{1}{2} \partial_x (h_1 u_2), \quad (3.36b)$$

$$0 = -\frac{1}{2} h_1 \partial_x p_1 - h \partial_x p_2 + 4 \partial_x (h S) - \frac{\mu}{h_1} u_2, \quad (3.36c)$$

$$0 = (1 + \lambda_{21} \partial_t + \lambda_{21} u_2 \partial_x) S - (1 + \lambda_{22} \partial_t + \lambda_{22} u_2 \partial_x) \partial_x u_2. \quad (3.36d)$$

196 where

$$p_1 = -(\sigma + 1) \partial_{xx} h_1 - \partial_{xx} h, \quad \text{and} \quad p_2 = -\partial_{xx} h_1 - \partial_{xx} h + \phi'(h). \quad (3.37)$$

## 4 Newtonian liquid layers with large viscosity ratios

For the special case when  $\lambda_{21} = \lambda_{22} = 0$  the upper liquid layer is a purely viscous fluid and we obtain the thin-film model

$$\partial_t h = -\partial_x (h u_2), \quad (4.1a)$$

$$\partial_t h_1 = \frac{1}{12\mu} \partial_x (h_1^3 \partial_x p_1) - \frac{1}{2} \partial_x (h_1 u_2), \quad (4.1b)$$

$$0 = -\frac{1}{2} h_1 \partial_x p_1 - h \partial_x (p_2 + \phi'(h)) + 4 \partial_x (h \partial_x u_2) - \frac{\mu}{h_1} u_2. \quad (4.1c)$$

Interestingly, also the thin-film model (4.1) has not been considered before. Thin-film two-layer models that have been investigated in the literature, such as in [1, 35] or more recently in [23], considered only the case when the viscosity ratios  $\mu_1/\mu_2$  of the two liquids are of  $O(1)$ .

This model is also instructive as it will be used to derive an expression for an apparent slip, and compare to the dynamics of single layer dewetting films from a solid substrate. Moreover, it serves to contrast the behaviour of dewetting viscoelastic films, which we investigate in the last section.

### 4.1 Transitions in flow regimes

We investigate first the morphologies and dynamics of dewetting rims as they occur after the top layer ruptures. In particular, we contrast the results for the thin-film model for which  $\mu_1/\mu_2 = O(1)$  with those for which  $\mu_1/\mu_2 = O(\varepsilon^2)$ , that we have derived in the previous section.

For moderate viscosity ratios, the resulting model has been derived previously derived in [1, 35] or in [23]. When we set the slip parameters in (3.5) in [23] to zero we obtain the system

$$\partial_t \mathbf{h} = \partial_x (Q \cdot \partial_x \mathbf{p}), \quad (4.2a)$$

where  $\mathbf{h}$  denotes the vector  $(h_1(x, t), h(x, t))$ ,  $\mathbf{p} = (p_1(x, t), p_2(x, t))$ , and the mobility matrix  $Q$  is given by

$$Q = \frac{1}{\mu} \begin{bmatrix} \frac{h_1^3}{3} & \frac{h_1^2 h}{2} \\ \frac{h_1^2 h}{2} & \frac{\mu}{3} h^3 + h_1 h^2 \end{bmatrix}, \quad (4.2b)$$

with

$$\begin{aligned} \partial_x p_1 &= -\partial_x ((\sigma + 1) \partial_{xx} h_1 + \partial_{xx} h), \\ \partial_x p_2 &= -\partial_x (\partial_{xx} h + \partial_{xx} h_1 - \phi'(h)). \end{aligned}$$

From an asymptotic point of view, the two models correspond to two distinguished limits, and we expect an overlapping region of validity of (4.2) for small viscosity ratios  $\mu_1/\mu_2$  with (4.1) for large  $\mu$ . We present numerical results for each of the two models and different values for the viscosity ratios  $\mu_1/\mu_2$  and  $\mu$ , with a fixed choice for the remaining parameter  $\sigma = 1$ . Specifically, we set  $\mu_1/\mu_2 = 0.001, 1, 1000$  in (4.2) and  $\mu = 0.001, 1, 1000$  in (4.1).

We observe in fig. 2 that by changing the viscosity ratio in (4.2) the profile of the upper layer assumes for all values of  $\mu_1/\mu_2$  shows a rim with an oscillatory decay towards the undisturbed parts of the upper layer. The wavelength of the oscillation increases as the ratio  $\mu_1/\mu_2$  decreases.

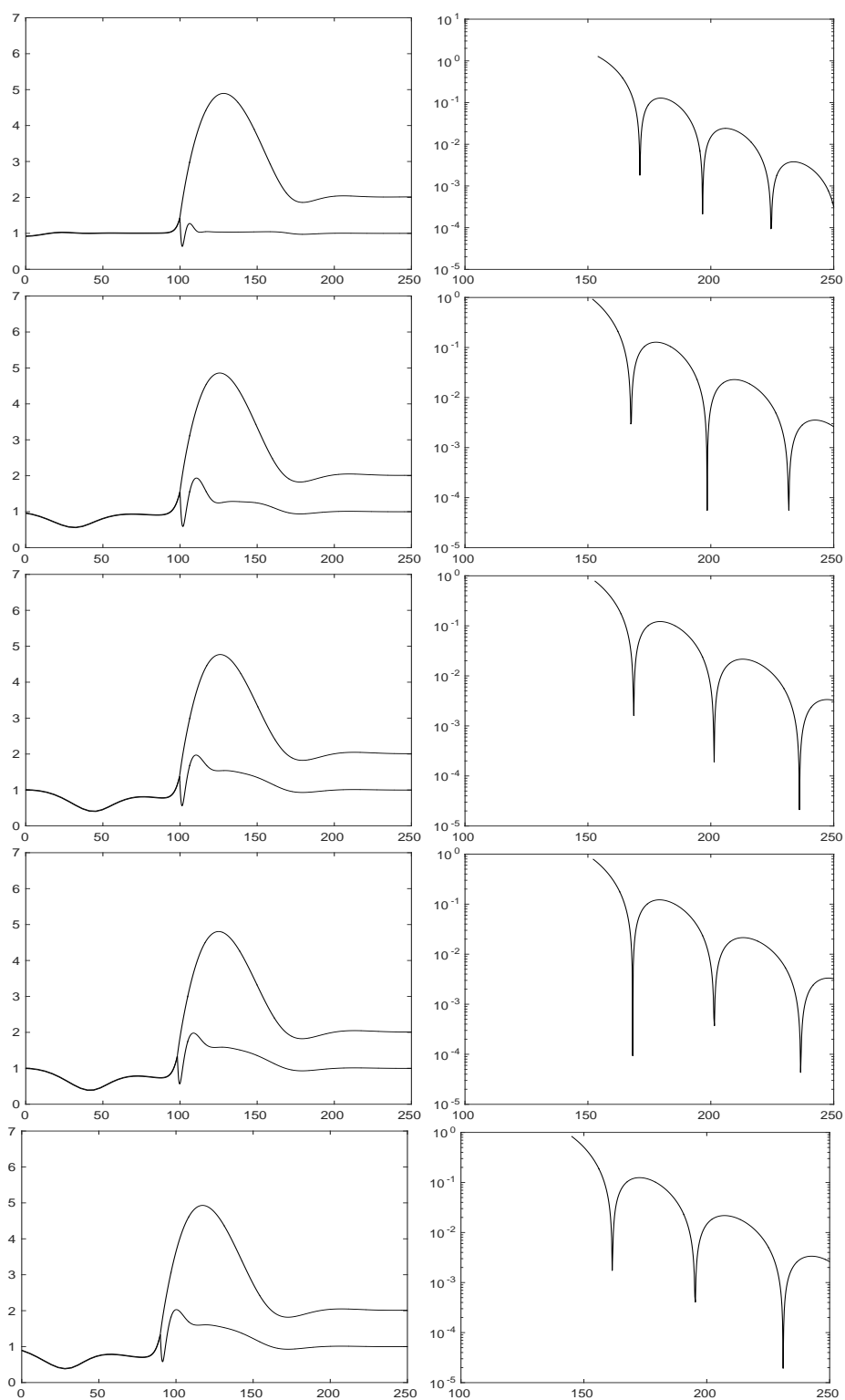


Figure 2: The moderate viscosity ratio model (4.2), with  $\mu_1/\mu_2 = 10, 1, 0.1, 0.01, 0.001$ , from top to bottom.

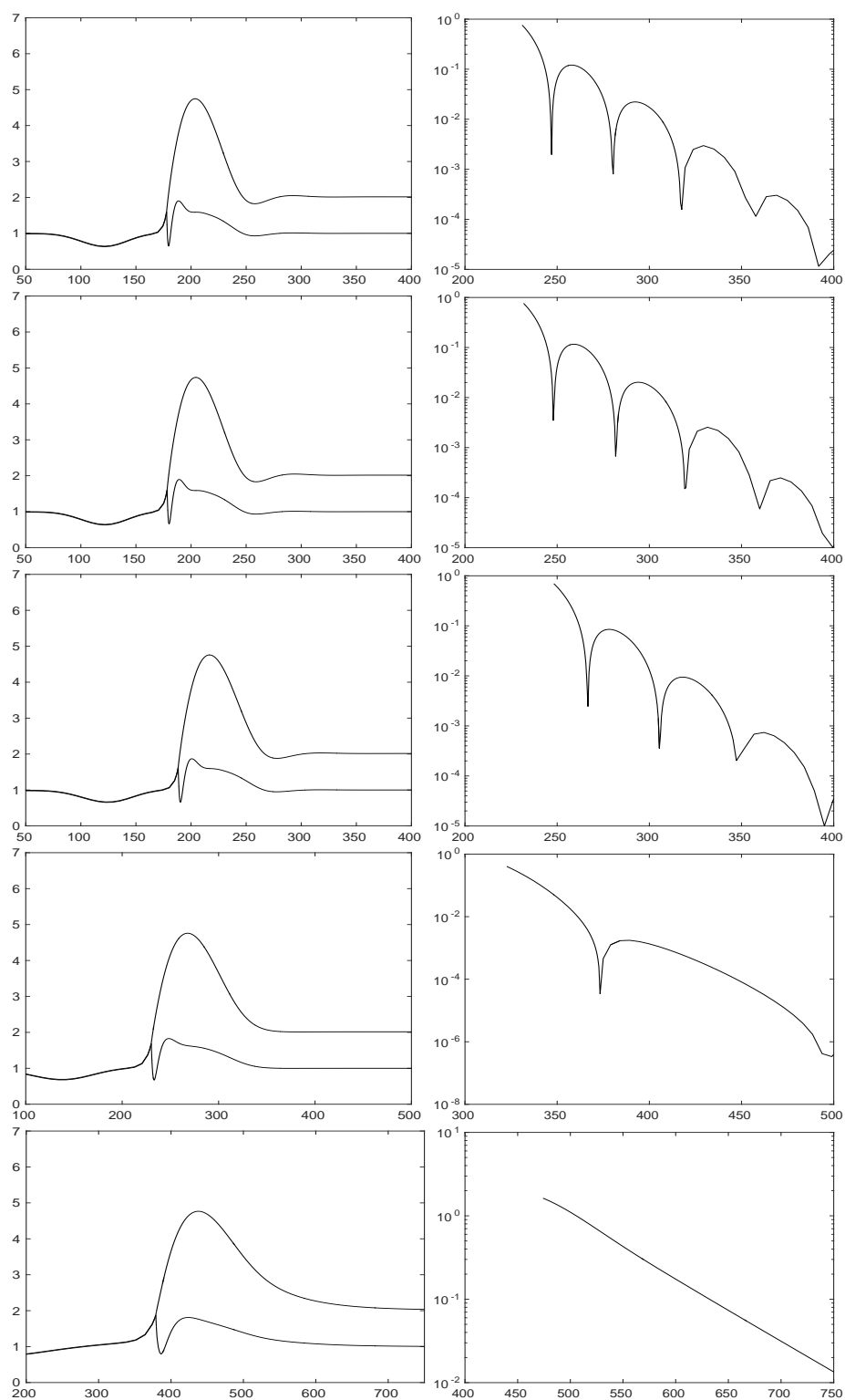


Figure 3: The small viscosity ratio model (4.1), with  $\mu = 10, 1, 0.1, 0.01, 0.001$ , from top to bottom.

At the same time the profile of the liquid-liquid interface  $h_1$  changes from almost no deviation from its equilibrium shape to a symmetric, to an unsymmetric profile, fig. 2 (bottom), with a more pronounced elevation near the dewetting front.

This tendency, of the unsymmetric shape of the  $h_1$  interface is dramatically increased even for the thin-film model (4.1), even for the largest viscosity ratio both the rim of the upper layer and the profile of the liquid-liquid interface have very pronounced asymmetric shapes. Moreover, as the value of the viscosity ratio is decreased in (4.1) the decay of the rims toward the undisturbed regions changes from oscillatory to a monotone behaviour as shown in fig. 3.

This characteristic change in profile has also been observed in the context of dewetting films from solid substrates that exhibit large slip [15, 33], where it was shown that, while keeping other parameters fixed, the slip length controls this morphological transition. In the next section we will explore the connection between the viscosity ratios in a two layer system and the apparent slip.

## 4.2 Connection to apparent slip

The situation we study here with two layers of very different thickness and viscosity indeed arises for polymer solutions due to the depletion of the polymer fraction near the wall [9], where it has been seen as a source for apparent slip. For reviews on sources of apparent slip from experimental and theoretical perspective we also refer to [13, 19, 34, 39, 42], where it is contrasted with the so-called effective slip, where the molecules adjacent to the wall are thought to move, possibly facilitated by the presence of surface roughness, while in the depletion scenario, slippage is due to the lubrication effect of the reduced viscosity in the depletion layer near the wall. Mechanisms for the molecular segregation have been investigated in [40] and [11, 12], alongside with estimates for the depletion length.

We also note that bi-viscosity models have also been introduced to explain the occurrence of slip between two strongly segregated homopolymers. These separate into two nearly pure bulk layers, so that mixing only occurs in a thin interfacial layer, where the viscosity is reduced to the repulsion between the inter-penetrating chains [18].

For polymer melts, the theory for the origin of slip is quite different and relates the slip length  $b$  to the length of the polymer chains  $N$  and the entanglement length  $N_e$  via  $b = aN^3/N_e^2$ , where  $a$  is a polymer specific molecular size. The proximity of the surface is thought to increase the effective entanglement length, so that a gradient in the material properties does arise but is not fundamental for the appearance of slip. On the other hand, the magnitude of slip can be greatly modified by grafting different polymer chains to the substrate [2, 15, 16, 18] This is somewhat reminiscent of the mixing between the two polymer liquids in [18] and one may speculate if a similar mechanism as there may lead to a difference in the effective viscosity near to and further away from the that could contribute to the overall slip experienced by the bulk liquid as in the bi-viscosity situation modelled here.

To establish the connection to apparent slip we will focus here on very thin liquid substrates. To investigate this regime we introduce the quantity  $b_1 := h_1/\mu$  and assume that

$$b_1 = O(1) \quad \text{and} \quad h_1, \mu \ll 1. \quad (4.3)$$

In this case we obtain from (4.1) the leading order equations

$$\partial_t h_2 = -\partial_x (h_2 u_2), \quad (4.4a)$$

$$0 = h_2 \partial_x (\partial_{xx} h_2 - V(h_2)) + 4\partial_x (h_2 \partial_x u_2) - \frac{u_2}{b_1}. \quad (4.4b)$$

263 These two equations for  $h$  and  $u_2$  are similar to the strong-slip lubrication model for the evolution  
 264 of a single thin film on a solid substrate, where  $b_1$  corresponds to the slip length. But in our case  
 265 the quantity  $b_1$  is not a constant. In fact it fulfils the transport equation

$$\partial_t b_1 = -\partial_x(b_1 u_2). \quad (4.4c)$$

266 On the other hand, if we assume that  $\sigma = \sigma^*/\mu^2$ , with  $\sigma^* = O(1)$ , we obtain the system

$$\partial_t h_2 = -\partial_x(h_2 u_2), \quad (4.5a)$$

$$0 = \frac{\sigma^*}{2} b_1 \partial_{xxx} b_1 + h_2 \partial_x(\partial_{xx} h_2 - V(h_2)) + 4\partial_x(h_2 \partial_x u_2) - \frac{u_2}{b_1}, \quad (4.5b)$$

$$\partial_t b_1 = -\frac{\sigma^*}{12} \partial_x(b_1^3 \partial_{xxx} b_1) - \partial_x(b_1 u_2). \quad (4.5c)$$

267 For  $\sigma^*$  very large the last equation implies that  $b_1 = B_1$  with a constant  $B_1$ . Hence,

$$\partial_t h_2 = -\partial_x(h_2 u_2), \quad (4.6a)$$

$$0 = h_2 \partial_x(\partial_{xx} h_2 - V(h_2)) + 4\partial_x(h_2 \partial_x u_2) - \frac{u_2}{B_1}. \quad (4.6b)$$

268 Carrying this out for the moderate viscosity ratio model (4.2), with  $m = \mu_1/\mu_2$ , and the  
 269 rescaling  $h_1 = mb_1$ , we obtain, for  $m \ll 1$ ,  $b_1 = O(1)$ , that

$$\partial_t h_2 = -\partial_x \left[ \left( \frac{1}{3} h^3 + b_1 h^2 \right) \partial_x (\partial_{xx} h_2 - V(h_2)) \right], \quad (4.7a)$$

$$\partial_t b_1 = -\partial_x \left[ \frac{b_1^2 h_2}{2} \partial_x (\partial_{xx} h_2 - V(h_2)) \right]. \quad (4.7b)$$

270 Again,  $b_1$  plays the role of an effective slip for the evolution of the top, i.e. liquid-air interface.

271 If we assume strong surface tension by also letting  $\sigma = \sigma^*/m^2$ , with  $\sigma^* = O(1)$ , we obtain in  
 272 the limit  $m \rightarrow 0$ ,

$$\partial_t h_2 = -\partial_x \left[ \sigma^* \frac{b_1^2 h_2}{2} \partial_{xxx} b_1 + \left( \frac{1}{3} h^3 + b_1 h^2 \right) (\partial_{xx} h_2 - V(h_2)) \right] \quad (4.8a)$$

$$\partial_t b_1 = -\partial_x \left[ \sigma^* \frac{b_1^3}{3} \partial_{xxx} b_1 + \frac{b_1^2 h_2}{2} \partial_x (\partial_{xx} h_2 - V(h_2)) \right]. \quad (4.8b)$$

273 If, in fact,  $\sigma^*$  is large, this reduces to  $b_1 = B_1$  with a constant  $B_1$ , and

$$\partial_t h_2 = \left[ \left( \frac{1}{3} h^3 + \frac{1}{4} B_1 h^2 \right) \partial_x (\partial_{xx} h_2 - V(h_2)) \right]. \quad (4.9)$$

274 Quantitative accuracy of our estimate of the effective slip can be obtained in particular for  
 275 the large  $\mu$  case, by verifying that for a given far-field value of  $b_1 = h_1/\mu$  the transition from  
 276 an oscillatory to a monotonic profile  $h_2$  or vice-versa occurs for (4.1) and (4.4) under identical  
 277 conditions. In fig. 4 we have chosen  $h_1$  and  $\mu$  such that  $b_1$  is in the order of magnitude of  $\beta$   
 278 compared to the results in [33]. We obtain a transition from oscillatory to monotonic profiles for  
 279 the top layer in the numerical solutions of (4.1), similarly to the results in [33] (fig. 8) for the  
 280 strong-slip model with the corresponding  $\beta = b_1$ .

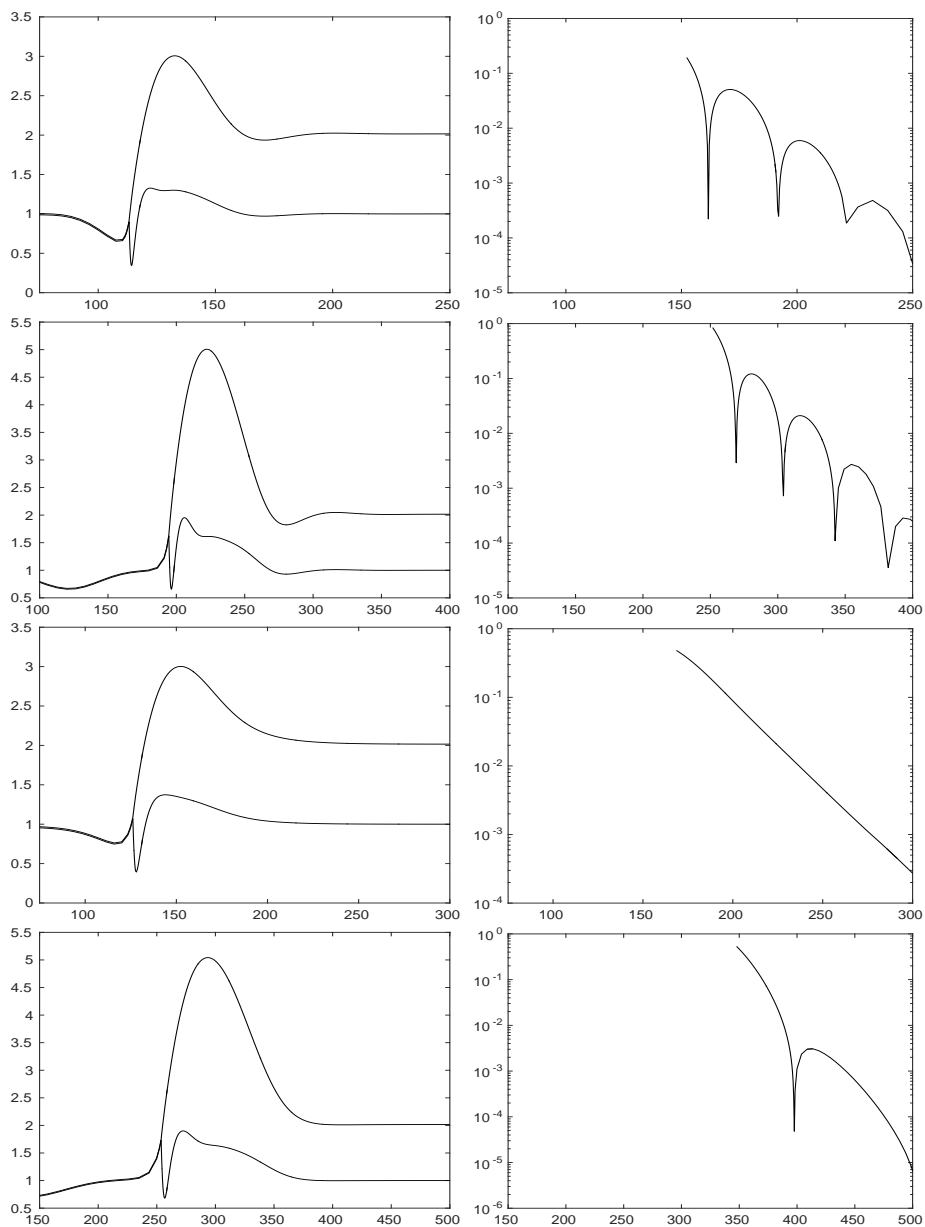


Figure 4: The small viscosity ratio model (4.1), top row :  $\mu = 1$ , morphology (left) and semilogy (right), early stage; 2nd row: top row :  $\mu = 1$ , morphology (left) and semilogy (right), later stage; 3rd row :  $\mu = 0.01$ , morphology (left) and semilogy (right), early stage; bottom row: top row :  $\mu = 0.01$ , morphology (left) and semilogy (right), later stage.

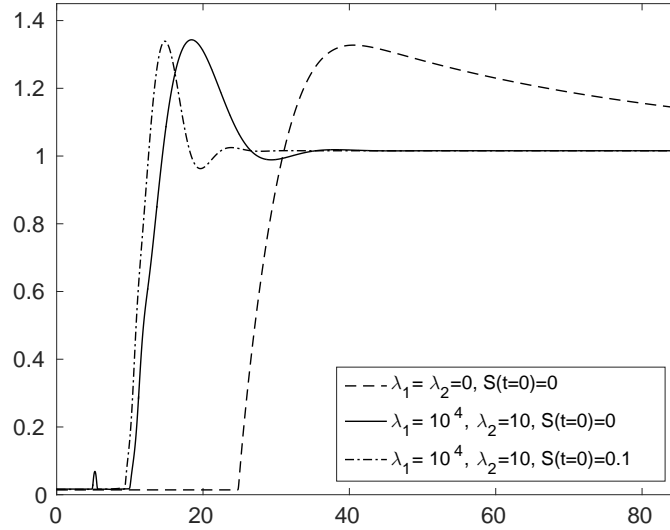


Figure 5: The strong-slip, viscoelastic model on a solid substrate (5.1), comparison of the morphologies for different values of  $\lambda_1$ ,  $\lambda_2$  and initial conditions for  $S$ .

## 5 Dewetting viscoelastic films: dynamics and morphology

281

We now return to the dewetting thin film problem with a corotational Jeffreys' model. There are a number of theoretical and experimental studies concerning the morphologies and dewetting rates of single layer viscoelastic dewetting films [3, 5, 22], in particular the period after rupture and in stressed state, for example due to prior spin coating process [38, 41, 44]. Our models enable to simulate the fully nonlinear viscoelastic behaviour for different parameter choices. Here we give a few illustrations for large values of  $\lambda_{21}$  and in particular compare dynamics and morphologies to the Newtonian model.

In the previous section we showed a strong connection of the small viscosity ratio model (4.1) to the strong-slip model on a solid substrate. Obviously, a similar derivation can be carried out in the viscoelastic case. In fact, considering the same limit in (3.36) one ends up with

289

$$\partial_t h_2 = -\partial_x(h_2 u_2), \quad (5.1a)$$

$$0 = h_2 \partial_x(\partial_{xx} h_2 - \phi'(h_2)) + 4\partial_x(h_2 \partial_x u_2) - \frac{u_2}{B_1}, \quad (5.1b)$$

$$0 = (1 + \lambda_1 \partial_t + \lambda_1 u_2 \partial_x) S - (1 + \lambda_2 \partial_t + \lambda_2 u_2 \partial_x) \partial_x u_2. \quad (5.1c)$$

The latter model can be found for example in [5].

292

In order to distinguish the impact of the viscoelastic rheology from the influence of a deformable liquid substrate on the morphology of a dewetting film after rupture, it is instructive to first consider the case of the viscoelastic film dewetting from a solid substrate. The latter case is also interesting since its rupture and subsequent dewetting dynamics has not been investigated before within a thin-film framework.

293

As a first example we compare in fig. 5 an early stage of the dynamics given by (5.1) for  $B_1 = 600$ . In the case  $\lambda_1 = \lambda_2 = 0$  we observe the expected asymmetric shape of the rim, where the maximum of the rim is connected to the the undisturbed film by an almost straight line. This behaviour changes if one includes viscoelastic effects. To illustrate this we have chosen

294

295

296

297

298

299

300

301



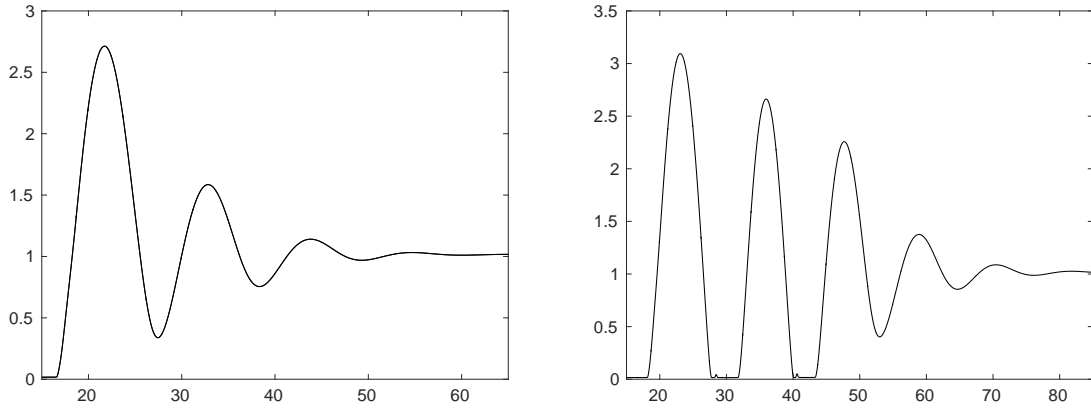


Figure 6: The strong-slip, viscoelastic model on a solid substrate (5.1), morphologies for large  $\lambda_1$  at two different times.

302  $\lambda_1 = 10000$  and  $\lambda_2 = 10$ . We can make several interesting observations. First, the shape of the  
 303 rim attains the form of a parabola similar to the one obtained in the weak -slippage case. Another  
 304 immediate observation is that the dewetting rate of the contact line is significantly slower in the  
 305 viscoelastic case. Finally, we see that the first two effects are enhanced when the initial value of  
 306 the quantity  $S$  is non-zero, which means that we impose a non-zero initial stress. Here we have  
 307 chosen the value  $S(t = 0, x) \equiv 0.1$ .

308 In fig. 6 the evolution of the case with non-zero initial  $S$  is shown. We observe that while  
 309 the dewetting rim grows, it quickly pinches off, forming a new constactline. Hence, instead of a  
 310 retracting film we observe that a series of droplets is formed. Moreover, for certain parameter  
 311 settings, also smaller secondary droplets pinch off just before the new contact line forms and is  
 312 a result of a non-zero initial stress. In the case of  $S(t = 0, x) \equiv 0$  the rim retracts while remaining  
 313 stable.

314 Next, we consider the corresponding situation for the bi-layer model, i.e. we consider (3.36)  
 315 with a very low viscosity ratio and a small initial thickness of the liquid substrate; here we chose  
 316  $\mu = 1/6000$  and  $h_1(t = 0, x) \equiv 0.1$ . In fig. 7 we observe almost the same behaviour as in fig. 5.  
 317 In the Newtonian case, the asymmetric rim shape is obtained, while in the two viscoelastic cases  
 318 the rim attains a more parabolic shape. Also here we encounter that the contact line moves much  
 319 slower in the presence of viscoelastic effects. In fig. 8 we again observe that for  $S(t = 0, x) \equiv 0.1$   
 320 there is an immediate formation of droplets. However, there are some differences in the size of  
 321 the droplets compared to the case of an solid substrate. In particular, the smaller secondary  
 322 droplets are larger than in 6.

323 While these examples can only provide a first glimpse into the rich dynamic and morphological  
 324 structure of the evolving viscoelastic films, a systematic parameter study is the topic of an  
 325 upcoming investigation.

## 326 6 Conclusion

327 In this work we derived conditions that allow an asymptotically consistent reduction of governing  
 328 free boundary problem for a two-layer liquid system to a thin-film model with fully nonlinear  
 329 viscoelastic rheology, such as the corotational Jeffreys' model. These conditions show that this

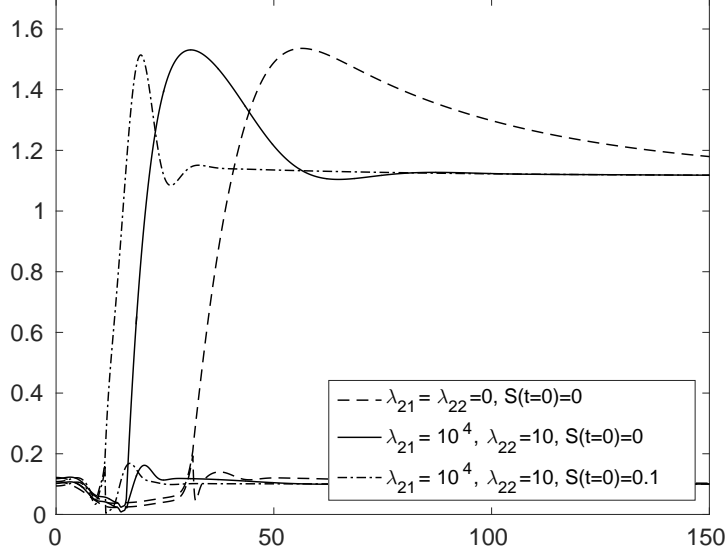


Figure 7: The small viscosity ratio, viscoelastic model (3.36), comparison of the morphologies for different values of  $\lambda_1$ ,  $\lambda_2$  and initial conditions for  $S$ .

330 is controlled by the order of magnitude of the viscosity ratio of the liquid bi-layer.

331 We also revisited the Newtonian case and showed that in this case the corresponding thin-film  
 332 model reduces to model similar in structure to the so-called strong-slip model for the one layer  
 333 situation. In particular, also here, the well-known transition [15] from oscillatory to monotone  
 334 decay of the rim tail for increasing slip lengths can also be observed for the bi-layer, here for  
 335 decreasing viscosity ratio. Similarly, as done in [33] one can capture this transition using a linear  
 336 stability analysis about the undisturbed upper layer.

In summary, when linearising (4.1), using the ansatz

$$h_1 = a + \exp(\alpha\zeta), \quad h = 1 + \chi \exp(\alpha\zeta), \quad \zeta = x - s(t),$$

337 two equations for  $\chi$ , can be obtained and  $\sigma$  for given  $\dot{s}(t)$ . A non-trivial solution for  $\chi$  only exists  
 338 if the coefficient matrix vanishes. This gives a high-order (up to 8th order) polynomial equation  
 339 for  $\sigma$ .

$$\dot{s} - \dot{s} \frac{a}{2} \chi = \frac{a^3}{12\mu} ((\sigma + 1)\alpha^3 + \chi\alpha^3), \quad (6.1)$$

$$0 = \frac{a^2}{2} ((\sigma + 1)\alpha^3 + \chi\alpha^3) + a(\alpha^3 + \chi\alpha^3 - \phi\chi\alpha) + 4a\dot{s}\chi\alpha^2 - \mu\dot{s}\chi. \quad (6.2)$$

340 which then can be solved  $\sigma$ , where only the roots which have  $\text{Re } \sigma < 0$  are relevant so that  
 341  $\exp(\sigma\xi)$  decays as  $\chi \rightarrow \infty$ . One can then determine how many roots qualify under this criterion  
 342 and which of them have non-zero imaginary part or change their imaginary part from zero to  
 343 non-zero for varying  $\dot{s}$ .

344 We then exploited this fact to show that for the limiting case of a liquid substrate, that is  
 345 thin compared to the dewetting film on top, an expression for an apparent slip can be derived.

346 Our numerical simulations on dewetting viscoelastic films shortly after the rupture process  
 347 and using stressed initial conditions showed that, by varying the time relaxation parameters  $\lambda_{21}$

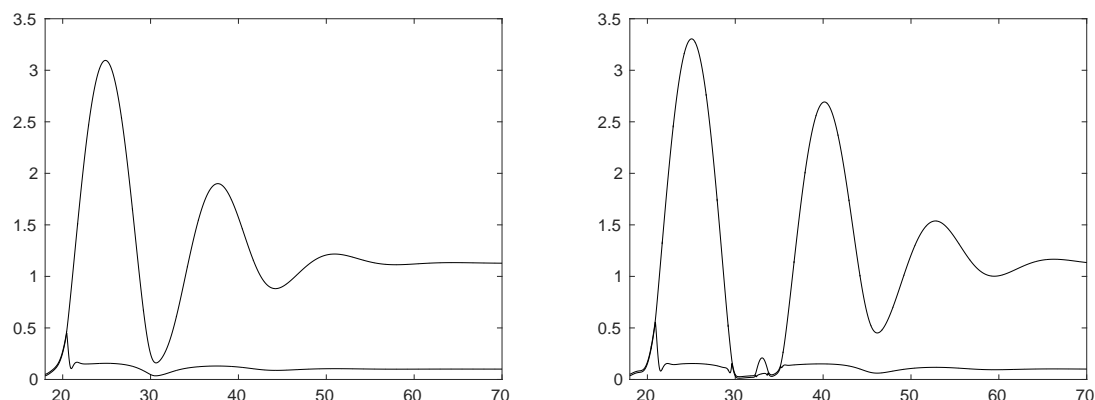


Figure 8: The small viscosity ratio, viscoelastic model (3.36), morphologies for large  $\lambda_1$  at two different times.

348 and  $\lambda_{22}$  rather surprising new morphologies can be obtained. They reveal that in the limiting  
 349 Newtonian case the ri shows a particular asymmetric shape as has been shown for dewetting liquid  
 350 films with large slip for the single layer case. In contrast for increasing  $\lambda_{12}$  these asymmetric  
 351 morphology is relaxed but other new structures emerge. This is also accompanied by varying  
 352 dewetting regimes. An intriguing morphology for large  $\lambda_{12}$  shows pinch off of the tail of the rim  
 353 and a structure reminiscent to the “beads on a string” structure observed before in viscoelastic  
 354 (Oldroyd-B) strings, see for example [29, 31]. These and further regimes will be investigated  
 355 systematically in an upcoming work.

## 356 Acknowledgements

357 SJ gratefully acknowledges the support by the DFG of the project “Structure formation in thin  
 358 Bi-layers” within the priority programme SPP 1506 “Transport at Fluidic Interfaces”. The  
 359 authors would also like to thank Tobias Ahnert for fruitful discussions on the numerics.

## 360 References

- 361 [1] D. Bandyopadhyay, R. Gulabani, and A. Sharma. Instability and dynamics of thin liquid  
 362 bilayers. *Ind. Eng. Chem. Res.*, 44(5):1259–1272, 2005.
- 363 [2] O. Bäumchen, R. Fetzer, and K. Jacobs. Reduced interfacial entanglement density affects  
 364 the boundary conditions of polymer flow. *Phys. Rev. Lett.*, 103:247801, 2009.
- 365 [3] O. Bäumchen and K. Jacobs. Slip effects in polymer thin films. *Journal of Physics: Con-*  
 366 *densed Matter*, 22(3):033102, 2010.
- 367 [4] K. Binder and H. L. Frisch. Interfacial profile between coexisting phases of a polymer  
 368 mixture. *Macromolecules*, 17(12):2928–2930, 1984.
- 369 [5] R. Blossey. Viscoelastic thin films. In *Thin Liquid Films*, Theoretical and Mathematical  
 370 Physics, pages 89–115. Springer Netherlands, 2012.

- 371 [6] R. Blossey, A. Münch, M. Rauscher, and B. Wagner. Slip vs. viscoelasticity in dewetting  
372 thin films. *Eur. Phys. J. E - Soft Matter*, 20:267–271, 2006.
- 373 [7] F. Brochard-Wyart, G. Debregeas, R. Fondecave, and P. Martin. Dewetting of supported  
374 viscoelastic polymer films: Birth of rims. *Macromolecules*, 30:1211–1213, 1997.
- 375 [8] F. Brochard-Wyart, P. Martin, and C. Redon. Liquid/liquid dewetting. *Langmuir*,  
376 9(12):3682–3690, 1993.
- 377 [9] J. Cayer-Barrioz, D. Mazuyer, A. Tonck, and E. Yamaguchi. Drainage of a Wetting Liquid:  
378 Effective Slippage or Polymer Depletion? *Tribology Letters*, 32(2):81–90, 2008.
- 379 [10] R. V. Craster and O. K. Matar. On the dynamics of liquid lenses. *J. Colloid and Interface  
380 Sci.*, 303:503–506, 2006.
- 381 [11] P. G. de Gennes. Polymer solutions near an interface. 1. adsorption and depletion layers.  
382 *Macromolecules*, 14:1637–1644, 1981.
- 383 [12] P. G. de Gennes. Polymers at an interface: a simplified view. *Advances in Colloid and  
384 Interface Science*, 27(3):189–209, 1987.
- 385 [13] B. V. Derjaguin and N. V. Churaev. Structure of water in thin layers. *Langmuir*, 3:607–612,  
386 1987.
- 387 [14] A. D. F. Dunbar, P. Mokarian-Tabari, A. J. Parnell, S. J. Martin, M. W. A. Skoda, and  
388 R. A. L. Jones. A solution concentration dependent transition from self-stratification to  
389 lateral phase separation in spin-cast PS:d-PMMA thin films. *Eur. Phys. J. E - Soft Matter*,  
390 31:369–375, 2010.
- 391 [15] R. Fetzer, K. Jacobs, A. Münch, B. Wagner, and T. P. Witelski. New slip regimes and the  
392 shape of dewetting thin liquid films. *Phys. Rev. Lett.*, 95:127801, 2005.
- 393 [16] R. Fetzer, A. Münch, B. Wagner, M. Rauscher, and K. Jacobs. Quantifying Hydrodynamic  
394 Slip: A Comprehensive Analysis of Dewetting Profiles. *Langmuir*, 23(21):10559–10566, 2007.
- 395 [17] L. S. Fisher and A. A. Golovin. Instability of a two-layer thin liquid film with surfactants:  
396 Dewetting waves. *J. Colloid and Interface Sci.*, 307(1):203–214, 2007.
- 397 [18] J. L Goveas and G. H Fredrickson. Apparent slip at a polymer-polymer interface. *Eur.  
398 Phys. J. B - Condensed Matter and Complex Systems*, 2(1):79–92, 1998.
- 399 [19] S. Granick, Y. Zhu, and H. Lee. Slippery questions about complex fluids flowing past solids.  
400 *Nature Materials*, 2:221–227, 2003.
- 401 [20] S. Y. Heriot and A. L. Jones. An interfacial instability in a transient wetting layer leads to  
402 lateral phase separation in thin spin-cast polymer-blend films. *Nature Materials*, 4:782–786,  
403 2005.
- 404 [21] S. Herminghaus, K. Jacobs, and R. Seemann. Viscoelastic dynamics of polymer thin films  
405 and surfaces. *Eur. Phys. J. E*, 12(1):101–110, 2003.
- 406 [22] S. Herminghaus, R. Seemann, and K. Jacobs. Generic morphologies of viscoelastic dewetting  
407 fronts. *Phys. Rev. Lett.*, 89(5):056101, 2002.
- 408 [23] S. Jachalski, D. Peschka, A. Münch, and B. Wagner. Impact of interfacial slip on the stability  
409 of liquid two-layer polymer films. *J. Engr. Math.*, 86(1):9–29, 2014.

- 410 [24] J.-F. Joanny. Wetting of a liquid substrate. *Physicochemical Hydrodynamics*, 9(1-2):183–196,  
411 1987.
- 412 [25] M. B. Jones, D. L. S. McElwain, G. R. Fulford, M. J. Collins, and A. P. Roberts. The effect  
413 of the lipid layer on tear film behaviour. *Bull. Math. Biol.*, 68:1355–1381, 2006.
- 414 [26] R. E. Khayat. Transient two-dimensional coating flow of a viscoelastic fluid film on a  
415 substrate of arbitrary shape. *J. Non-Newton. Fluid Mech.*, 95(2–3):199–233, 2000.
- 416 [27] P. E. King-Smith, B. A. Fink, J. J. Nichols, K. K. Nichols, R. J. Braun, and G. B. McFadden.  
417 The contribution of lipid layer movement to tear film thinning and breakup. *IOVS*, 50:2747–  
418 2756, 2009.
- 419 [28] J. J. Kriegsmann and M. J. Miksis. Steady motion of a drop along a liquid interface. *SIAM*  
420 *Journal of Applied Mathematics*, 64(1):18–40, 2003.
- 421 [29] J. Li and M. A. Fontelos. Drop dynamics on the beads-on-string structure for viscoelastic  
422 jets: A numerical study. *Physics of Fluids*, 15(4):922–937, 2003.
- 423 [30] G. M. Homsy M. A. Spaid. Stability of newtonian and viscoelastic dynamic contact lines.  
424 *Physics of Fluids*, 8(2):460–478, 1996.
- 425 [31] G. H. McKinley. Visco-elasto-capillary thinning and break-up of complex fluids. *Submitted*  
426 *to Annual Rheology Reviews*, 2005.
- 427 [32] A. Münch, B. Wagner, M. Rauscher, and R. Blossey. A thin-film model for corotational  
428 jeffreys fluids under strong slip. *Eur. Phys. J. E*, 20(4):365–368, 2006.
- 429 [33] A. Münch, B. Wagner, and T. P. Witelski. Lubrication models with small to large slip  
430 lengths. *J. Engr. Math.*, 53:359–383, 2006.
- 431 [34] C. Neto, D. R. Evans, E. Bonaccorso, H.-J. Butt, and V. S. J. Craig. Boundary slip in  
432 newtonian liquids: a review of experimental studies. *Rep. Prog. Phys.*, 68:2859–2897, 2005.
- 433 [35] A. Pototsky, M. Bestehorn, D. Merkt, and U. Thiele. Morphology changes in the evolution  
434 of liquid two-layer films. *The Journal of chemical physics*, 122:224711, 2005.
- 435 [36] O. Hassager R. B. Bird, R. C. Armstrong. *Dynamics of Polymeric Fluids (Vol. 1)*. Wiley  
436 & Sons, New York, 1977.
- 437 [37] M. Rauscher, A. Münch, B. Wagner, and R. Blossey. A thin-film equation for viscoelastic  
438 liquids of jeffreys type. *Eur. Phys. J. E*, 17(3):373–379, 2005.
- 439 [38] G. Reiter, M. Sferrazza, and P. Damman. Dewetting of thin polymer films at temperatures  
440 close to the glass transition. *Eur. Phys. J. E*, 12(1):133–138, 2003.
- 441 [39] J. Sanchez-Reyes and L. A. Archer. Interfacial slip violations in polymer solutions: role of  
442 microscale surface roughness. *Langmuir*, 19:3304–3312, 2003.
- 443 [40] R. Tuinier and T. Taniguchi. Polymer depletion-induced near an interface. *J. Phys. Condens.*  
444 *Matter*, 17:L4–L9, 2005.
- 445 [41] T. Vilmin and E. Raphael. Dewetting of thin viscoelastic polymer films on slippery sub-  
446 strates. *Europhysics Letters*, 72:781, 2005.

- 447 [42] O. I. Vinogradova. Slippage of water over hydrophobic surfaces. *Int. J. Miner. Process*,  
448 56:31–60, 1999.
- 449 [43] Y. L. Zhang, O. K. Matar, and R. V. Craster. Surfactant spreading on a thin weakly  
450 viscoelastic film. *J. Non-Newton. Fluid Mech.*, 105(1):53–78, 2002.
- 451 [44] F. Ziebert and E. Raphaël. Dewetting of thin polymer films: Influence of interface evolution.  
452 *Europhysics Letters*, 86(4):46001, 2009.